A simulation study of helicopter ship landing procedures incorporating measured flow-field data

D G Thomson*, **F Coton,** and **R Galbraith**
Department of Aerospace Engineering, University of Glasgow, Glasgow, UK

The manuscript was received on 17 March 2005 and was accepted after revision for publication on 27 July 2005.

DOI: 10.1243/095441005X30351

Abstract: The aim of this article is to investigate the use of inverse simulation to help identify those regions of a ship's flight deck which provide the safest locations for landing a rotorcraft in various atmospheric conditions. This requires appropriate information on the wind loading conditions around a ship deck and superstructure, and for the current work, these data were obtained from wind tunnel tests of a ship model representative of a typical helicopter carrier/assault ship. A series of wind tunnel tests were carried out on the model in the University of Glasgow's 2.65 × 2.04 m wind tunnel and three-axis measurements of wind speed were made at various locations on the ship deck. Measurements were made at four locations on the flight deck at three different heights. The choice of these locations was made on the basis of preliminary flow visualization tests which highlighted the areas where the most severe wind effects were most likely to occur. In addition, for the case where the wind was from 30° to starboard, measurements were made at three further locations to assess the extent of the wake of the superstructure. The generated wind profiles can then be imposed on the inverse simulation, allowing study of the vehicle and pilot response during a typical landing manoeuvre in these conditions. The power of the inverse simulation for this application is demonstrated by a series of simulations performed using configurational data representing two aircraft types, a Westland Lynx and a transport helicopter flying an approach and landing manoeuvre with the worst atmospheric conditions applied. It is shown from the results that attempting to land in the area aft of the superstructure in a 30° crosswind might lead to problems for the transport configuration due to upgusts in this area. Attempting to perform the landing manoeuvre in an aggressive manner is also shown to lead to diminished control margin in higher winds.

Keywords: inverse simulation, wind tunnel testing, deck landing

1 INTRODUCTION

The current world political situation has necessitated the development of rapid reaction forces usually required to be deployable from ships. The requirement for helicopters (combat and transport) to be able to operate from ship decks in extremely difficult conditions (and possibly at night) has therefore emerged. The situation is made more difficult due to the airwake around the ship interacting with the helicopter rotors (main and tail). The nature of the airwake is determined by the geometry of the ship, and hence, each ship and helicopter combination has its own operational limits of permissible wind speed and direction for safe helicopter operation. This is often presented on a ship–helicopter operational limits (SHOL) diagram which is constructed by test flying the helicopter to and from the ship with the prevailing wind from various directions [**1, 2**]. Figure 1, reproduced from reference [**2**], shows a typical example of a SHOL diagram. Apart from the expense involved in doing these tests for each aircraft type likely to operate from the ship, it does of course mean that both the helicopter and the ship must be available for the tests. Therefore, it is clear that simulation methods, which might reduce the number of test flights required, would be advantageous. Lee *et al.* [**3**] describe one such method which uses CFD generated flow-field data

**Corresponding author: Department of Aerospace Engineering, University of Glasgow, Glasgow G12 8QQ, UK.*

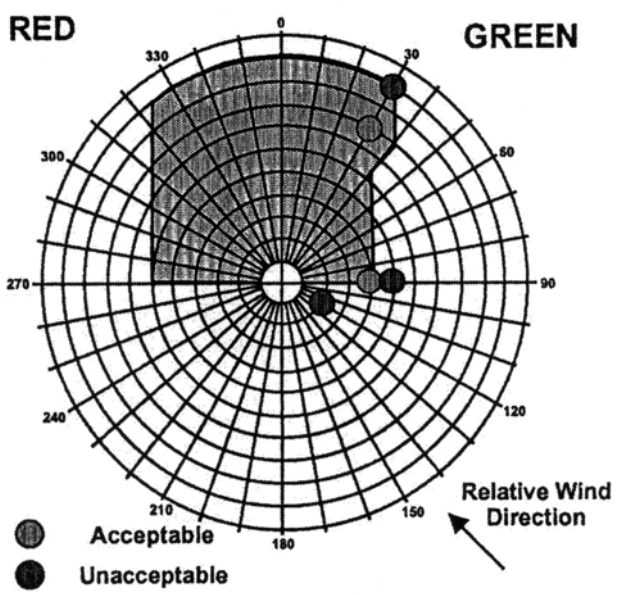

Fig. 1 A typical SHOL diagram (reproduced from reference [**2**])

and link this to a simulation model of the helicopter with an optimal control model of the pilot. In this article, a simulation method is demonstrated, which can be used to indicate wind speed and directions which will cause degradation of control margin for a given helicopter and ship combination. This method is therefore a powerful tool for the ship designer to ensure the basic design of the flight deck is 'helicopter friendly' and also as an aid in reducing the number of flights necessary to construct a SHOL diagram.

The method used here is known as 'inverse simulation', which involves specifying the manoeuvre which is to be flown and computing the control strategy and resulting response of the simulated helicopter. This is a technique which is finding increasing application [**4–6**], but much of the work in developing it and applying it to practical problems has been performed at Glasgow [**7–10**]. The main focus of this work has been the development of the helicopter inverse simulation package, Helinv. This package features a wide range of manoeuvre descriptions (the inputs to the simulation), allowing simulation of many operational scenarios and a non-linear, generic rotorcraft model. Owing to its generic construction, the helicopter model has a level of sophistication which allows valid simulation of a range of single main and tail rotor configurations. Allied with the wide range of manoeuvre descriptions, this makes Helinv a powerful tool for flight dynamics research.

The main advantage in adopting the inverse approach is that it is possible to set precise performance goals, then use the simulation to determine first if the simulated vehicle is capable of achieving the goals, and if so, what performance margin remains. Placing this in the context of the current application, the first stage is to define the flight path trajectory of interest – a mathematical description of a landing manoeuvre is required. Inverse simulation can then be used to determine the control inputs required by a subject helicopter flying the manoeuvre. This exercise in itself is useful as it is possible to vary aircraft and manoeuvre parameters to optimize the aircraft design or flying strategy adopted. The real power of the method is apparent when an atmospheric model is applied to the simulation. There is then the potential to simulate landing manoeuvres in the most severe atmospheric conditions. The atmospheric model could be a simple step or '1-cos' gust profile, but for the current study, data from wind tunnel tests of a model of a typical aircraft carrier shape have been used to generate realistic wind profiles. The wind tunnel tests were used to identify areas on the flight deck where potential difficulties on landing may arise due to local wind conditions caused by adverse aerodynamic effects from the ship airwake. Inverse simulation was then used to simulate a typical ship-borne helicopter landing through this wind profile.

In section 2, the inverse simulation package Helinv and the helicopter mathematical model embedded in it are described. The enhancement of the simulation to include a ship landing manoeuvre and atmospheric disturbances are presented in sections 3 and 4 along with the presentation of a typical simulation result. Section 5 of the article describes the wind tunnel testing of a ship model and discusses the results obtained. The synthesis of this data into the inverse simulation is presented in section 6. The simulations are repeated for a transport helicopter in section 7 which demonstrates how this technique might assist in the preparation of SHOL diagrams.

2 THE INVERSE SIMULATION PACKAGE HELINV

The conventional method of solving the Euler equations of motion is to use numerical integration to obtain vehicle response to given inputs. This method is well known and understood unlike the inverse method. Consequently, it is appropriate that a brief description of some of the basics to be included here (a fully detailed account of the method is presented in reference [**6**]).

2.1 The inverse algorithm

Essentially, the rates of change of the states in the equations of motion are calculated by numerical

differentiation (forward differencing). Effectively, the differential equations of motion become algebraic in form and can be solved, in the case of Helinv, by a Newton–Raphson approach.

The simulation is initiated by establishing the mathematical description of the manoeuvre of interest. This is in the form of time histories of four variables: three positions (x_e, y_e, z_e) and heading (ψ). This is easy to understand when one considers that the helicopter has four controls; hence four states may be constrained: main rotor collective pitch (θ_0) influences vertical motion (z_e), longitudinal cyclic pitch (θ_{1s}) fore and aft motion (x_e), lateral cyclic pitch (θ_{1c}) sideward motion (y_e), whereas tail rotor collective (θ_{0tr}) influences heading (ψ).

There are seven equations of motion, the six Euler rigid body equations

$$m\dot{U} = -m(WQ - VR) + X - mg \sin \Theta \tag{1}$$

$$m\dot{V} = -m(UR - WP) + Y + mg \cos \Theta \sin \Phi \tag{2}$$

$$m\dot{W} = -m(VP - UQ) + Z + mg \cos \Theta \cos \Phi \tag{3}$$

$$I_{xx}\dot{P} = (I_{yy} - I_{zz})QR + I_{xz}(\dot{R} + PQ) + L \tag{4}$$

$$I_{yy}\dot{Q} = (I_{zz} - I_{xx})RP + I_{xz}(R^2 - P^2) + M \tag{5}$$

$$I_{zz}\dot{R} = (I_{xx} - I_{yy})PQ + I_{xz}(\dot{P} - QR) + N \tag{6}$$

and the engine torque equation

$$\ddot{Q}_E = \frac{1}{\tau_{e_1}\tau_{e_2}}[-(\tau_{e_1} + \tau_{e_3})\dot{Q}_E - Q_E + K_3(\Omega - \Omega_{idle} + \tau_{e_2}\dot{\Omega})] \tag{7}$$

where τ_{e_1}, τ_{e_2}, τ_{e_3}, K_3 are the time constants and gain of the governor and Ω_{idle} is the angular velocity of the rotor in idle.

Once cast in algebraic form, these equations are solved at regular, discrete time intervals through the manoeuvre for the seven unknowns: θ_0, θ_{1s}, θ_{1c}, and θ_{0tr} (the control displacements), the roll and pitch attitudes (Φ and Θ), and the rotorspeed Ω. The pilot's stick displacements (η_0, η_{1s}, η_{1c}, and η_{0tr}) are then readily obtained from the known calibration relationships with the blade displacements. Of course, in calculating the control displacements, a wide range of other computations takes place, including power, torque, attitude, etc., giving a large amount of information on the aircraft's performance as it completes the manoeuvre. In this study, the control angles (i.e. blade angular displacements) are converted to stick positions for ease of interpretation.

2.2 The helicopter mathematical model

The mathematical model used by the inverse simulation Helinv is known as HGS (helicopter generic simulation) [**11**]. The main features of HGS include a multi-blade description of the main rotor with quasi-steady flapping assumed, dynamic inflow, an engine and rotorspeed governor model, and look-up tables for fuselage aerodynamic forces and moments. The question of the validity of the results is also important – if any meaningful information is to be derived, then the mathematical model must replicate the actions of the real aircraft. In the case of Helinv, comparisons have been made using trajectory data from manoeuvres flown by real helicopters to drive the inverse simulation. The computed states and controls are compared with those recorded in the flight tests to establish the validity of the simulation. The results have shown good correlation for a range of manoeuvres [**7**]; the validity for low speed manoeuvres such as the landing manoeuvres used in this work are particularly good. The HGS model is generic in structure, representing single main and tail rotor helicopters by a series of basic configurational parameters. It is then possible to simulate a wide range of different rotorcraft by developing appropriate data files for specific types.

3 INVERSE SIMULATION OF DECK LANDING

Figure 2 shows a schematic representation of a typical landing manoeuvre. It is assumed to begin with the helicopter keeping station with the ship from a position off its port side. The ship is travelling in a direction due north at a velocity V_s, with the helicopter positioned at a distance s to the side and height h above the landing point. The first phase of the manoeuvre involves a sidestep to a position over the deck; the helicopter is then stabilized and finally there is a vertical descent onto the deck itself. To obtain an inverse simulation of this manoeuvre, it is necessary to derive appropriate time histories of the aircraft position, relative to an earth fixed datum, and its heading ($x_e(t)$, $y_e(t)$, $z_e(t)$, $\psi(t)$). As the manoeuvre consists of a series of phases, it is natural to derive the manoeuvre model in the same way.

3.1 The sidestep phase

The origin is located at the starting point of the manoeuvre, and the sidestep phase is assumed to take a total time t_1. The helicopter moves sidewards picking up velocity until it reaches a maximum value $\dot{y}_{max}$ at a time $\frac{1}{2}t$. The sideward motion is then

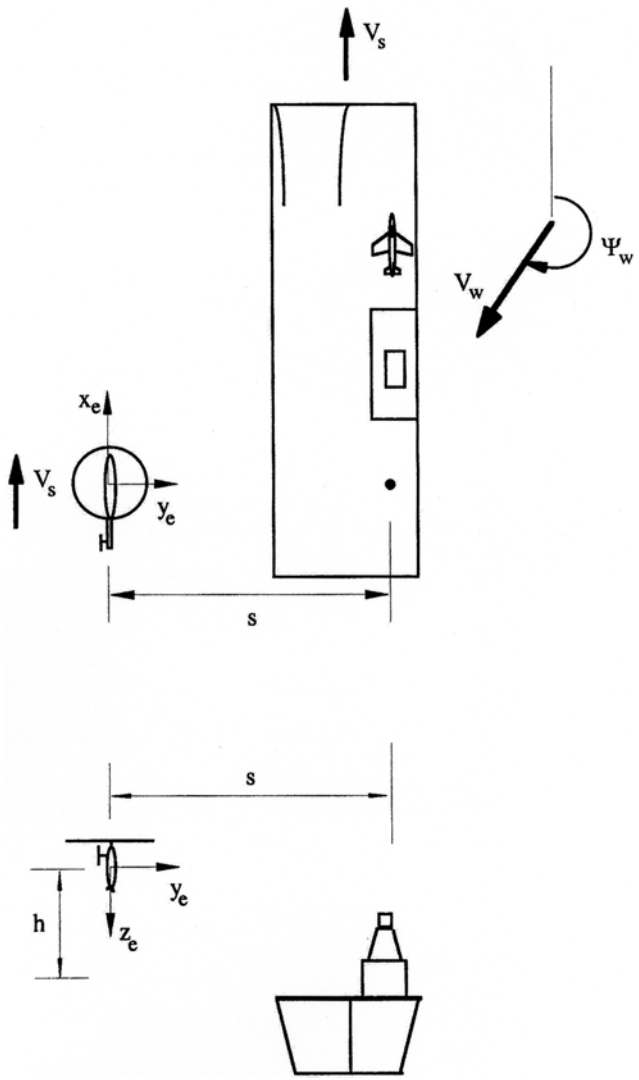

Fig. 2 Schematic representation of deck landing manoeuvre

arrested and the helicopter is brought to a hover over the landing spot. It has been shown [**12**] that this motion is best modelled by considering the sideward velocity profile, $\dot{y}_e(t)$. From this description, the following boundary conditions are proposed

$$\begin{array}{llll} t = 0 & \dot{y}_e(t) = 0 & \ddot{y}_e(t) = 0 & \dddot{y}_e(t) = 0 \\ t = \frac{1}{2}t_1 & \dot{y}_e(t) = \dot{y}_{\max} & & \\ t = t_1 & \dot{y}_e(t) = 0 & \ddot{y}_e(t) = 0 & \dddot{y}_e(t) = 0 \end{array}$$

The zero acceleration conditions at the beginning and end of the sidestep ensure that the aircraft is in trim at these points, and the third-order derivative condition is simply to ensure a required level of smoothness. The simplest mathematical function that satisfies these seven conditions is a sixth order polynomial

$$\dot{y}_e(t) = \left[-64\left(\frac{t}{t_1}\right)^6 + 192\left(\frac{t}{t_1}\right)^5 - 192\left(\frac{t}{t_1}\right)^4 + 64\left(\frac{t}{t_1}\right)^3 \right] \dot{y}_{\max} \tag{8}$$

This may seem to be an over simplification; however, previous work [**12**] in validation of this assumption shows a very good fit between this ideal velocity profile and those recorded from flight test. The sideward velocity, $\dot{y}_e(t)$, and distance, s, are related by the simple expression

$$\int_0^{t_1} \dot{y}_e(t)\mathrm{d}t = s \tag{9}$$

Substitution of equation (8) into equation (9) allows an analytical solution which yields

$$t_1 = \frac{50s}{23\dot{y}_{\max}} \tag{10}$$

Hence, it is possible to define the lateral position of the helicopter, s, and the maximum sideward velocity, $\dot{y}_{\max}$, calculate t_1 from equation (10), and hence generate a time history of sideward velocity, $\dot{y}_e(t)$, from equation (8).

3.2 Stabilization phase

It is assumed that once the helicopter reaches its position over the landing point, there will be a period of time, t_s, taken to stabilize the helicopter. In practise, this may be several seconds, but for simulation purposes only a few seconds are required.

3.3 Vertical descent phase

From the stabilized hover, the descent is initiated until some maximum vertical velocity, $\dot{z}_{\max}$, is reached. The descent is arrested and the aircraft brought to rest on the deck. If it is assumed that the maximum vertical velocity occurs half-way through this process, then it is clear that the same velocity profile as used for the sidestep will be suitable. If the descent takes a time t_d and the time base t^* is defined, where

$$t^* = t - (t_1 + t_s) \tag{11}$$

then the vertical velocity profile is given by

$$\dot{z}_e(t) = \left[-64\left(\frac{t^*}{t_d}\right)^6 + 192\left(\frac{t^*}{t_d}\right)^5 - 192\left(\frac{t^*}{t_d}\right)^4 + 64\left(\frac{t^*}{t_d}\right)^3 \right] \dot{z}_{max} \quad (12)$$

As with the sidestep phase, it is possible to calculate the duration of the descent from the height, h, and the maximum vertical velocity, $\dot{z}_{max}$

$$t_d = \frac{50h}{23\dot{z}_{max}} \quad (13)$$

Specifying h and $\dot{z}_{max}$ allows t_d to be calculated from equation, (13) and hence, the descent velocity time history, $\dot{z}_e(t)$, is defined from equation (12). The velocity profile for the complete manoeuvre is therefore as follows.

3.3.1 Sidestep phase ($0 < t < t_1$)

$$\dot{x}_e(t) = V_s$$

$$\dot{y}_e(t) = \left[-64\left(\frac{t}{t_1}\right)^6 + 192\left(\frac{t}{t_1}\right)^5 - 192\left(\frac{t}{t_1}\right)^4 + 64\left(\frac{t}{t_1}\right)^3 \right] \dot{y}_{max}$$

$$\dot{z}_e(t) = 0$$

3.3.2 Stabilization phase ($t_1 < t < (t_1 + t_s)$)

$$\dot{x}_e(t) = V_s \quad \dot{y}_e(t) = 0 \quad \dot{z}_e(t) = 0$$

3.3.3 Descent phase ($(t_1 + t_s) < t < (t_1 + t_s + t_d)$)

$$\dot{x}_e(t) = V_s$$

$$\dot{y}_e(t) = 0$$

$$\dot{z}_e(t) = \left[-64\left(\frac{t^*}{t_d}\right)^6 + 192\left(\frac{t^*}{t_d}\right)^5 - 192\left(\frac{t^*}{t_d}\right)^4 + 64\left(\frac{t^*}{t_d}\right)^3 \right] \dot{z}_{max}$$

Defining the manoeuvre in this way allows its severity to be prescribed by varying the parameters s, h, $\dot{y}_{max}$, and $\dot{z}_{max}$. For example, holding $\dot{y}_{max}$ constant and decreasing the distance s forces the helicopter to accelerate and decelerate more quickly to achieve the defined manoeuvre in a shorter time.

Finally, it is necessary to define the heading of the helicopter to complete the set of four constraints. In still air conditions, it is sufficient to make the assertion that $\Psi = 0$, that is, the aircraft heading is identical to that of the ship. In conditions of ambient wind, the pilot may, for example, choose to point the nose of the aircraft into the wind, effectively performing the manoeuvre with zero sideslip (i.e. $V = 0$). To give the flexibility required to model different flying techniques, it is necessary at this stage to simply say that

$$\Psi = f(t)$$

and the form of f is dependent on the strategy adopted by the pilot.

A typical manoeuvre description is shown in Fig. 3 where the parameters used were $V_s = 10$ knots, $s = 20$ m, $\dot{y}_{max} = 10$ knots, $h = 10$ m, $\dot{z}_{max} = 5$ m/s, and $t_s = 1$ s.

The $\dot{y}_e(t)$ plot ('ydot') shows an increase from zero to the maximum value, $\dot{y}_{max}$, of 5.148 m/s (10 knots) and back to zero over a time of 8.44 s (as calculated from equation (10)). There is then a 1 s stabilization period (t_s) and the vertical descent begins at 9.44 s ('zdot' plot). The maximum vertical velocity, $\dot{z}_{max}$, of 5 m/s is clearly visible and the aircraft touches down after a further 4.34 s, as calculated by equation (13), giving a manoeuvre time of 13.78 s. The $\dot{x}_e(t)$ plot ('xdot') shows a constant value of 5.148 m/s throughout the manoeuvre, which is equivalent to the 10 knots velocity of the ship. Integration of the velocities generates the flight path plots as shown.

The flight path parameters generated in the example shown in Fig. 3 have been applied to the inverse simulation Helinv with representative data for a Lynx helicopter (derived from Padfield [**13**]) applied to the helicopter mathematical model. The results are shown in Fig. 4. The manoeuvre is initiated by a pulse of lateral cyclic stick of around 5 per cent of its travel. The resulting roll-time history indicates a maximum roll angle of around 10°. Halfway through the sidestep, the roll direction is reversed to bring the helicopter to a halt directly above the landing point. A second pulse of lateral cyclic pitch is applied to achieve this. After the 1 s stabilization period (i.e. at 9.44 s), there is a rapid drop of collective of almost 20 per cent to initiate the descent, followed by a rapid increase of around 35 per cent to arrest the downward motion. Finally, the collective is returned to its initial value to complete the manoeuvre. As the manoeuvre involves sideward and descending flight, there are only small inputs to longitudinal cyclic pitch, and subsequently, very small changes in pitch attitude are predicted. There are, however, more substantial changes in pedal position (tail rotor collective). During the sidestep phase, the input of tail rotor collective is necessary to balance the sideward force generated

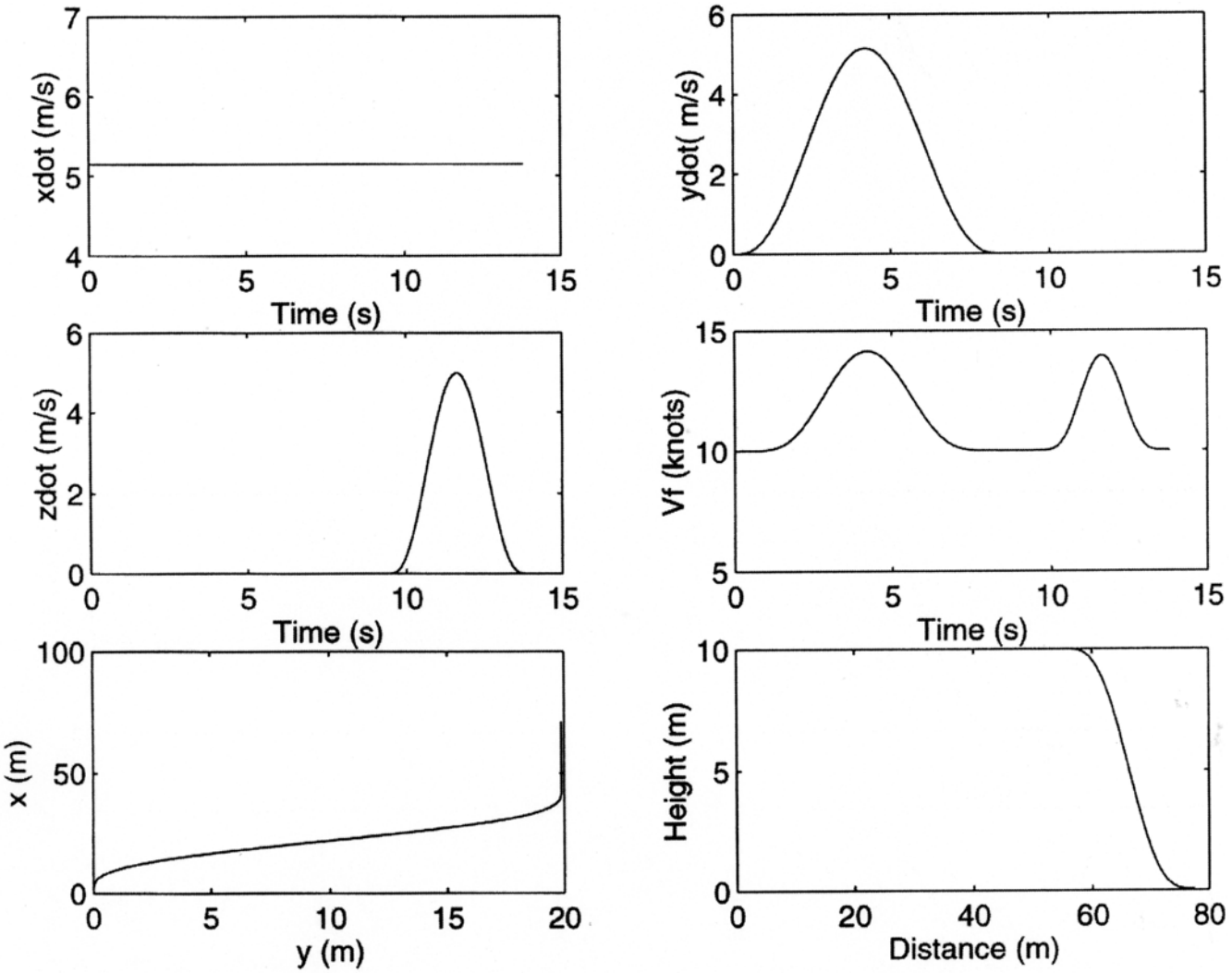

Fig. 3 Parameter time histories for modelled deck landing

by the lateral cyclic pitch, whereas during the descent, large inputs of main rotor collective have a bearing on the torque applied to the fuselage, and hence, there are large inputs of tail rotor collective to provide the anti-torque necessary to maintain heading.

The results shown in Fig. 4 are in still air conditions. In section 4, the changes necessary to the simulation to allow the inclusion of wind effects are detailed and results presented.

4 DECK LANDING IN PREVAILING WIND CONDITION

The HGS model had to be modified to enable the influence of prevailing wind on pilot strategy and vehicle behaviour to be evaluated. This study is particularly important as prevailing wind can significantly alter the power required and control margins of the helicopter, which when operating in confined spaces such as a ship flight deck can be crucial to the safety of the helicopter. A prevailing wind can also affect pilot strategy and is particularly important during the low speed phases of a landing manoeuvre where the pilot, for example, may find himself applying large degrees of sideslip to counteract the influence of a strong cross-wind. The modifications required for the mathematical model necessary to allow simulation of such conditions are presented in section 4.1. In this work, it is assumed that the aircraft is instantaneously immersed in the gust, that is, the effect of the rotor disc penetrating the gust is ignored.

4.1 Including the effects of atmospheric disturbances into the equations of motion

The aerodynamic forces and moments acting on a helicopter are generated by the relative motion of air over the vehicle. In inverse simulation, it is

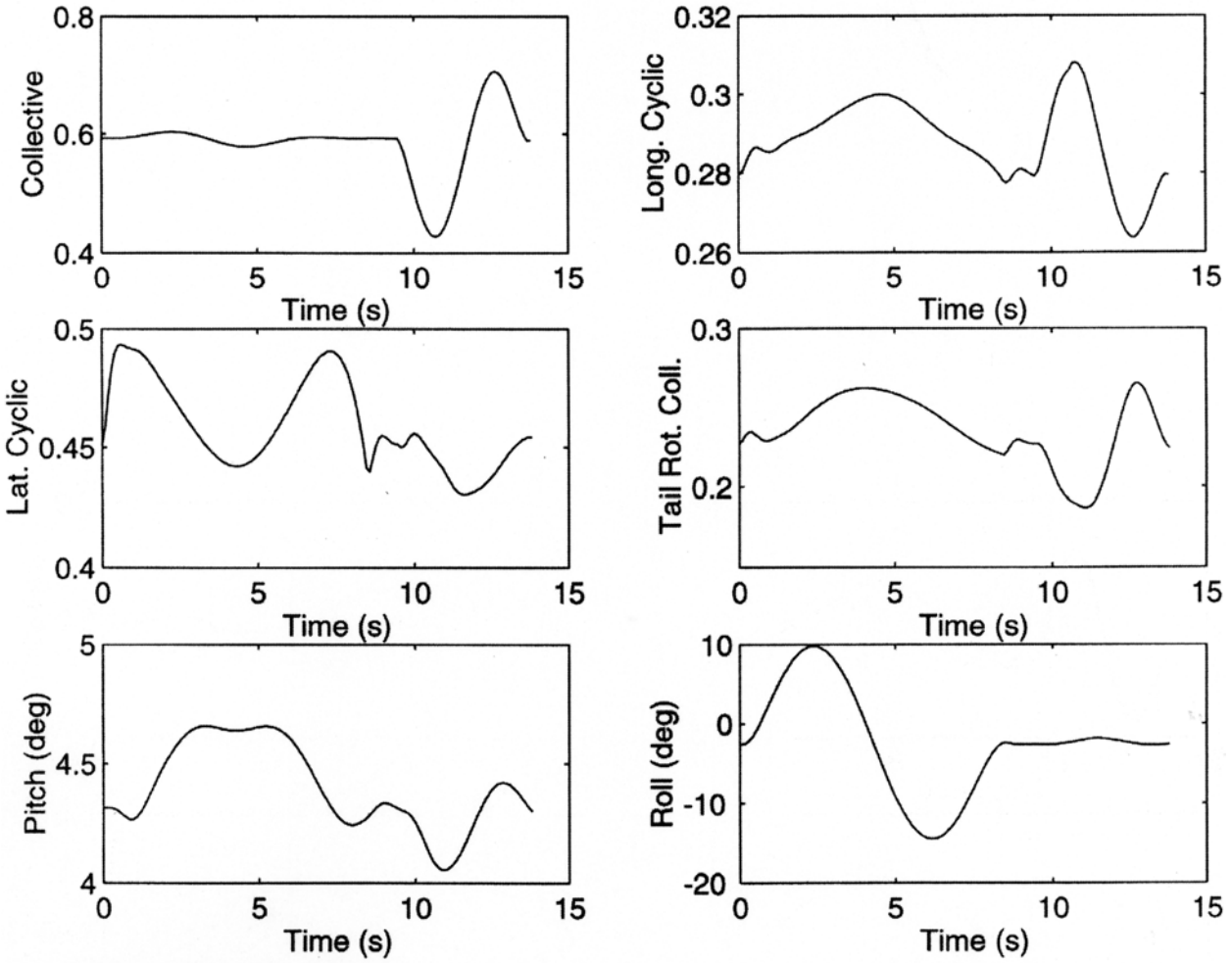

Fig. 4 Inverse simulation results for landing manoeuvre from Fig. 3, Lynx helicopter

usual for the vehicle's trajectory to be expressed with respect to some Earth fixed axes set, and previous investigations have assumed that the air surrounding the aircraft does not move relative to this axes set. The velocity time history of the helicopter may then be given by

$$\boldsymbol{V}_{\mathrm{h,g}} = \boldsymbol{V}_{\mathrm{h,a}} \tag{14}$$

where $\boldsymbol{V}_{\mathrm{h,g}}$ and $\boldsymbol{V}_{\mathrm{h,a}}$ denote the velocity vectors of the helicopter with respect to the ground and air, respectively.

Considering the influence of the prevailing wind, it is assumed that the wind velocity field is constant in the region in which the helicopter is immersed. Consequently, there are no significant wind speed variations over the rotor. Let $\boldsymbol{V}_{\mathrm{a,g}}$ denote the velocity vector of the air with respect to the ground; then, equation (14) can be rewritten as

$$\boldsymbol{V}_{\mathrm{h,g}} = \boldsymbol{V}_{\mathrm{h,a}} + \boldsymbol{V}_{\mathrm{a,g}} \tag{15}$$

As the velocity of the wind with respect to the ground is known, then the velocity of the helicopter with respect to the air can be easily determined from

$$\boldsymbol{V}_{\mathrm{h,a}} = \boldsymbol{V}_{\mathrm{h,g}} - \boldsymbol{V}_{\mathrm{a,g}} \tag{16}$$

The specification of the wind velocity is simplified if the horizontal components (in the earth axes x_{e}–y_{e} plane) and vertical components are considered separately. The wind velocity in the earth axes x_{e}–y_{e} plane is defined in terms of its absolute velocity component, V_{w}, and angle between the in-plane velocity vector and the x-axis denoted by Ψ_{w}, as illustrated in Fig. 2. With this definition, the wind directions are

$\Psi_{\mathrm{w}} = 0^{\circ}$ tailwind
$\Psi_{\mathrm{w}} = 90^{\circ}$ wind from port side
$\Psi_{\mathrm{w}} = 180^{\circ}$ headwind
$\Psi_{\mathrm{w}} = 270^{\circ}$ wind from starboard

The specification of the wind velocity is completed by defining the vertical component of wind, $\boldsymbol{V}_{w_v}$, and this is chosen to be positive downwards. Hence, the three wind velocity components of the vector $\boldsymbol{V}_{a,g}$ can be obtained from

$$\boldsymbol{V}_{a,g} = \begin{bmatrix} -\boldsymbol{V}_w \cos \Psi_w \\ -V_w \sin \Psi_w \\ \boldsymbol{V}_{w_v} \end{bmatrix}$$

Therefore, once the earth components of wind are known, the velocity of the helicopter with respect to air expressed in Earth axes may be determined from equation (16). It is then a simple matter to transform the resulting velocities through the Euler sequence (Ψ, Θ, Φ) to determine the velocity of the airflow with respect to helicopter in vehicle body axes. The aerodynamic components of wind velocity atthe rotorcraft centre of gravity, U_a, V_a, and W_a, are the sum of the inertial velocities, U, V, and W, and the wind components $U_{a,g}$, $V_{a,g}$, and $W_{a,g}$. Thus

$$U_a = U + U_{a,g}$$
$$V_a = V + V_{a,g}$$
$$W_a = W + W_{a,g}$$

The fuselage angle of incidence and sideslip used to determine the fuselage forces and moments can be given by

$$\alpha_F = \tan^{-1}\left(\frac{W_a}{U_a}\right) \quad \text{and} \quad \beta_F = \sin^{-1}\left(\frac{V_a}{V_f}\right)$$

where the flight velocity is given by $V_f = \sqrt{U_a^2 + V_a^2 + W_a^2}$. Hence, the aerodynamic forces and moments for the complete aircraft may be evaluated in the usual manner.

4.2 Inverse simulation of deck landing with a prevailing wind

Referring to Fig. 2, it is necessary to define a wind from a direction, Ψ_w, with constant velocity, V_w. Figure 5 shows inverse simulation results for a Westland Lynx helicopter flying the landing manoeuvre, described by Fig. 3, in still air (as in Fig. 4), in a constant 40 knot headwind (i.e. $\Psi_w = 180^\circ$ and $V_w = 40$ knots) and in a constant 40 knot tailwind (i.e. $\Psi_w = 0^\circ$ and $V_w = 40$ knots). It is assumed that there is no vertical component of the wind.

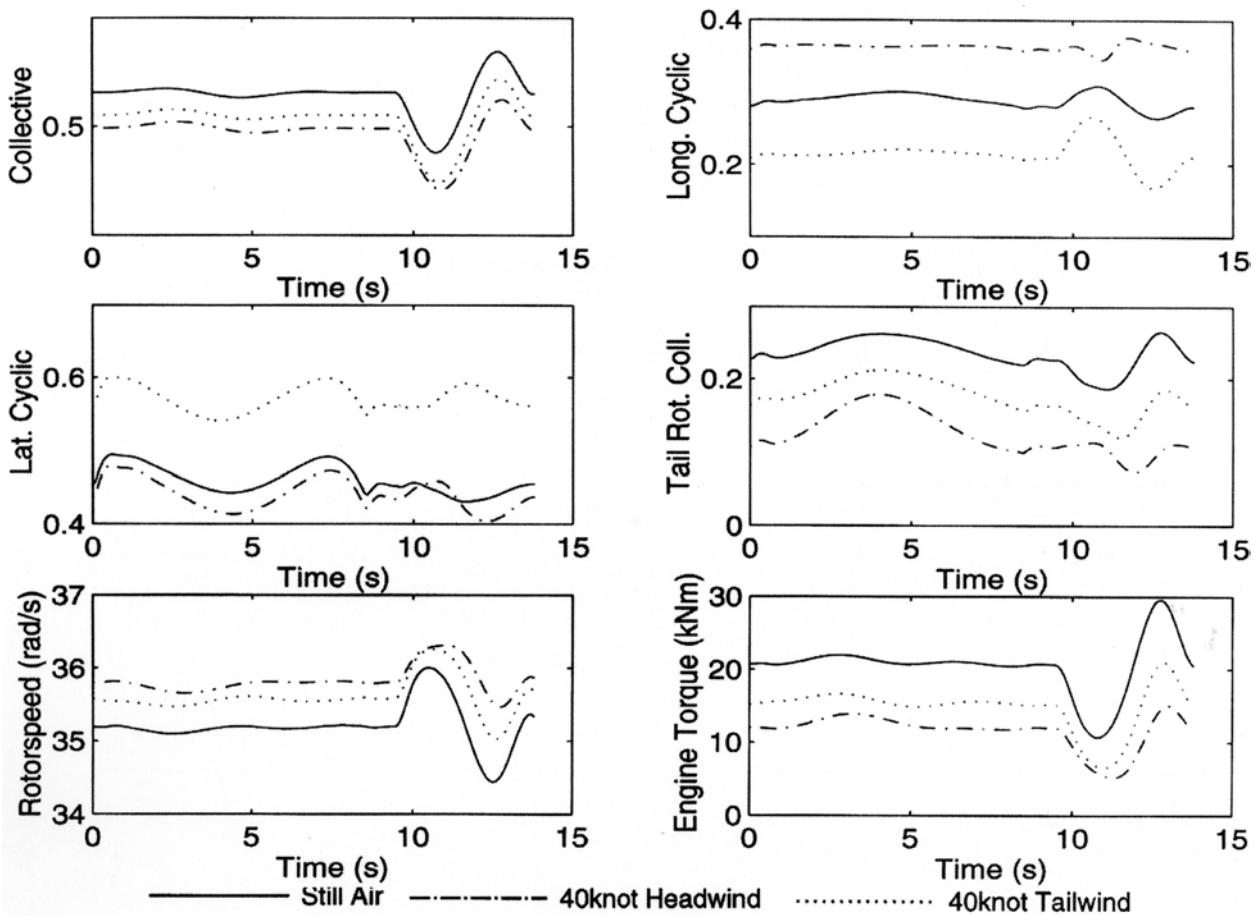

Fig. 5 Inverse simulation results for landing manoeuvre from Fig. 4 – fore/aft wind cases

The effect of flying the manoeuvre in a constant wind is quite clear – all the controls are offset from their still air values. The additional 40 knots airflow over the rotor gives a lower collective pitch to generate the same thrust, and hence, the requirements on engine torque and power are also reduced. The offset in longitudinal cyclic pitch indicates a forward motion of the stick to maintain fore/aft position relative to the ship in the 40 knot headwind and an aft motion for the tailwind case. Lower engine torque allows a reduction in tail rotor pitch, and hence, a shift in the lateral cyclic stick (less side force is required to counteract the tail rotor thrust).

There is nothing in Fig. 5 to suggest that landing in a constant headwind would cause a problem. There is ample control margin, with all the controls well within their limits as are engine and tail rotor torque. This is not a surprising result as landing into the wind is always the most desirable option. The power of an inverse simulation is that this manoeuvre can now be repeated with any wind intensity and direction applied. The simulation performed for Fig. 5 was repeated with the same wind intensity (40 knots) but with the focus on beam winds (i.e. $\Psi_w = 90^\circ$, 270°), and the results are plotted in Fig. 6.

A beam wind has two significant effects: it influences sideforce on the fuselage and the tail rotor inflow and hence thrust. Consider the case of the 40 knot wind from the port side (the chained line). As indicated in Fig. 2, it is assumed that the manoeuvre is initiated from the port side of the ship. The initial sideward motion is aided by the wind, and hence, a lower collective position is adopted when compared with the no wind case; however, in attempting to arrest the sideward motion as the ship deck is approached, the additional drag has to be countered by increased collective. This contrasts with the starboard wind case where additional collective is required to initiate the manoeuvre and less to achieve the 'hover' over the deck. The sideforce problem due to the beam wind will of course have an effect on required lateral cyclic position. The main problem with the beam wind is the effect it

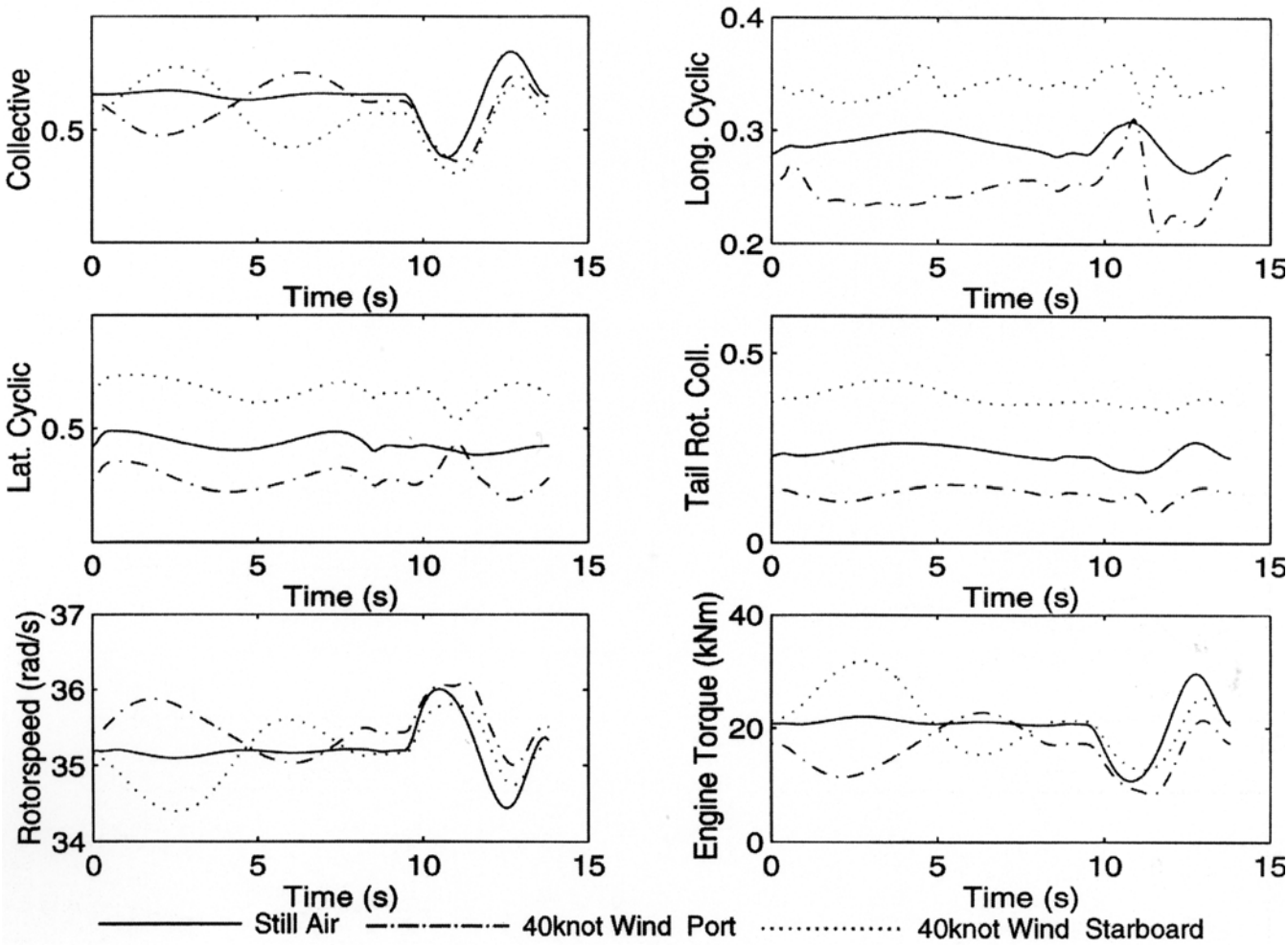

Fig. 6 Inverse simulation results for landing manoeuvre from Fig. 4 – beam wind cases

can have on tail rotor thrust. Consider the case of the Lynx where the main rotor rotates in an anti-clockwise direction when viewed from above, generating a torque in the clockwise direction on the fuselage. The tail rotor provides a thrust to port to generate the anti-torque moment (in an anti-clockwise direction) to this. A wind from the port direction (chained line) in addition to the port direction of motion can cause a reduction of the inflow and hence thrust generated, thereby leading to higher tail rotor collective pitch displacements. The value of 0.5 for tail rotor collective corresponds to the pedals being centralized, whereas a value of 0 corresponds to full left pedal. Figure 6 shows that with a starboard wind, there is plenty of control margins available on the pedals, whereas with a port wind causes a larger left pedal input, taking it close to its limits.

Another feature of these results is that the engine torque exceeds its maximum value between 2.11 and 3.52 s (coinciding with maximum collective pitch) in the starboard wind case. The simulation is predicting that the Lynx would not be able to fly this manoeuvre under these conditions – a reduced maximum sideward velocity or increased lateral distance from the ship at initiation of the manoeuvre would be necessary.

The use of inverse simulation to investigate the effect of a constant wind on deck landings has been demonstrated. Clearly, the situations of a beam wind are more critical than head or tail winds. Further, only constant winds were considered in this section. The real issue for helicopter and ship designers is the effect of flying the helicopter in airwake generated by a wind impinging on a ship superstructure. There is no limitation on the profile of the wind distribution applied to the inverse simulation, and so, it is possible to apply realistic atmospheric situations to the simulation. In the following section, results of a wind tunnel trial using a representative ship model are presented. These data are then used to generate realistic profiles for application to the simulation.

5 EXPERIMENTAL MEASUREMENT OF AIRWAKE AROUND MODEL OF AN ASSAULT SHIP

A series of wind tunnel tests were carried out on a model helicopter carrier/assault ship in the University of Glasgow's 2.65 × 2.04 m Argyll wind tunnel. The 1/145th scale ship model was made from wood and mounted on a ground board above the floor plane of the tunnel. Testing was conducted at a wind speed of 13.2 m/s giving a Reynolds number of 1.27 million (based on hull length), and

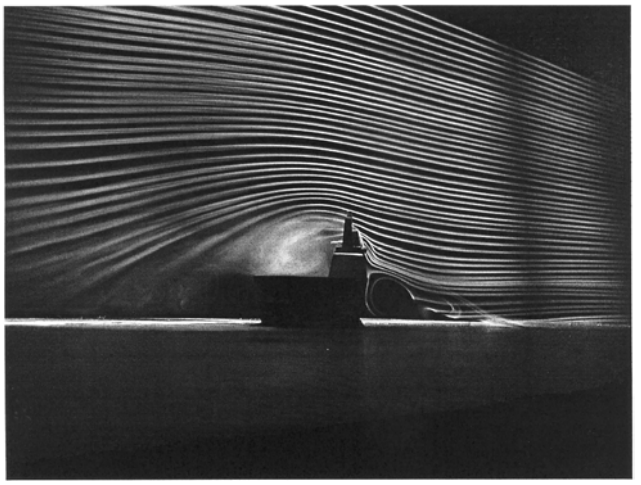

Fig. 7 Flow from 30° to starboard

three-component velocity measurements were made using a TSI IFA-300 Hot-Wire constant temperature anemometer system with DANTEC 55P61 cross-wire probes. These probes have 5 μm platinum plated tungsten wire sensors with a length to diameter ratio of 250. The measuring volume of the probes is approximately 0.8 mm in diameter and 0.5 mm in height. The test wind speed was chosen to allow the measuring system to resolve velocities over the full range of flow conditions expected around the ship.

A series of preliminary flow visualization tests were conducted on a smaller scale model of the ship in the University of Glasgow's 0.91 × 0.91 m smoke flow visualization facility. This study provided qualitative information that was then used to identify the most appropriate regions of the ship flow field to site the hot-wire sensors, i.e where the most severe wind effects were most likely to occur. An example of the visualization data is shown in Fig. 7 where a flow

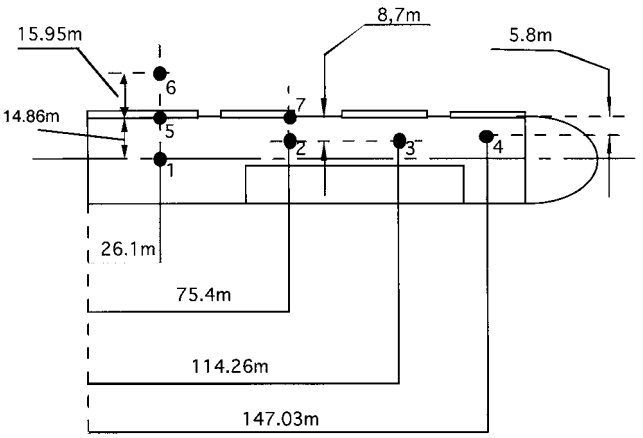

Fig. 8 Schematic representation of probe measurement positions

Table 1 Measurement heights above deck (full scale)

Height reference	Actual height (m)
1	22.2
2	14.8
3	7.4

from 30° to starboard is shown to produce a substantial recirculation region in the wake of the ship superstructure.

On the basis of the flow visualization study, hot-wire measurements were made at four locations on the flight deck at three different heights. The measurement locations used in the test are shown (in full scale) in Fig. 8, and the measurement heights are listed in Table 1 subsequently. In addition, for the case where the wind was from 30° to starboard, measurements were made at three further locations to assess the extent of the wake of the superstructure. In all cases, data were collected at a sampling rate of 1 kHz over a 4 s period. Prior to engaging in the full test programme, data were sampled at discrete locations around the ship over longer periods (up to 20 s) to determine the range of significant frequencies in the flow. On this basis, it was established that a 4 s measuring period was sufficient to provide accurate estimates of mean velocity.

The mean values of the measurements taken at these positions and heights are presented in Table 2. It should be noted that the velocities were measured relative to the flow direction, not the ship orientation. The sign convention of the velocities presented in Table 2 is as indicated in Table 3.

As accurate wind data are available for the locations and heights shown in Fig. 8 and Table 2, the focus here will be on creating flight path models which pass through these points and then superimposing the known wind conditions onto them. This technique will be illustrated first by considering the most severe case identified: a wind coming from an angle of 30° from starboard ($\Psi_w = 240°$) across the superstructure.

6 INVERSE SIMULATION OF LANDING IN WAKE FROM WIND ACROSS SUPERSTRUCTURE

The most severe wind condition identified from the wind tunnel tests was for locations aft of the

Table 2 Wind tunnel measurements of velocity

Run number	Wind direction (to starboard) (°)	Probe position	Probe height	U_f (m/s)	W_f (m/s)	V_f (m/s)
37	15	1	1	13.516	−2.148	0.463
38	15	1	2	8.506	−0.953	0.139
39	15	1	3	12.476	−1.059	0.759
40	15	2	1	12.476	−0.305	2.218
41	15	2	2	12.959	−0.394	2.801
42	15	2	3	9.887	−0.933	1.705
43	15	3	1	13.621	−1.123	0.478
44	15	3	2	13.825	−1.495	0.443
45	15	3	3	14.050	−1.616	0.959
46	15	4	1	13.322	−0.344	0.679
47	15	4	2	13.376	−0.300	0.281
48	15	4	3	13.481	−0.414	0.798
49	30	1	1	14.008	−2.127	−0.837
50	30	1	2	11.731	−1.515	−1.492
81	30	1	3	8.229	−0.129	−1.620
52	30	2	1	14.477	−2.691	1.399
53	30	2	2	10.522	−0.794	1.219
82	30	2	3	10.079	0.882	1.373
55	30	3	1	14.231	−1.668	0.031
56	30	3	2	14.495	−2.704	−0.306
83	30	3	3	12.303	−2.100	−0.115
58	30	4	1	13.597	−0.738	0.242
84	30	4	2	13.784	−1.055	1.322
85	30	4	3	14.017	−1.324	1.341
86	30	5	1	12.251	−2.178	1.463
87	30	5	2	6.648	−1.516	0.017
88	30	5	3	10.352	−0.382	0.855
89	30	6	1	13.562	−0.617	2.816
90	30	6	2	13.123	−0.349	3.551
91	30	6	3	11.723	1.472	2.290
92	30	7	1	13.979	−0.927	2.127
93	30	7	2	12.333	0.678	2.312
94	30	7	3	9.202	−0.401	1.000

Table 3 Velocity sign convention

Streamwise velocity, U_f	Positive downstream
Vertical velocity, V_f	Positive downwards
Cross-stream velocity, W_f	Positive to the left (looking downstream)

superstructure when a wind was present 30° from the starboard side. Measurements of wind velocities at points 6, 5, and 1 have been recorded for a height equivalent to 22.2 m and for two other heights at the landing point 1. The aim first is to derive a flight path model which passes through these points.

6.1 Construction of flight path

Referring to Fig. 8, the lateral distance travelled from point 6 to point 1 is 30.81 m, i.e. for the manoeuvre model(referring to section 3) $s = 30.81$ m. From Table 2, it is convenient to have the height above the deck as $(h =)$ 22.2 m, and retaining the other values for the manoeuvre (i.e. $V_s = 10$ knots, $\dot{y}_{max} = 10$ knots, $\dot{z}_{max} = 5$ m/s, $t_s = 1$ s), it is possible to construct the flight path as shown in Fig. 9.

All the inertial data are now available for the simulation; however, it is also necessary to superimpose the wind velocity profile on top of the manoeuvre. This profile has been measured in a positional coordinate frame from the wind tunnel test but is required as a time history for the simulation. Therefore, it is necessary to locate the time at which the measurement points are reached. These are indicated in Fig. 9, for example, having initiated the manoeuvre at point 6, point 5 which is a lateral distance of 15.95 m (Fig. 8) is reached after 6.8 s when using the model described in section 3.

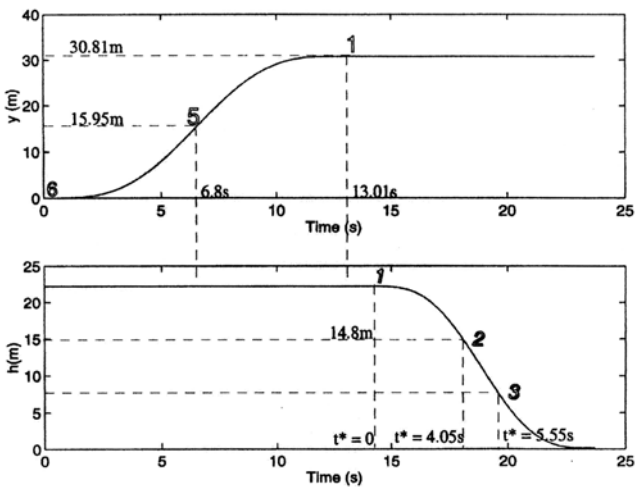

Fig. 9 Flight path for landing through points 6–5–1

6.2 Construction of wind profile

The atmospheric data for the simulation are required in relation to an earth fixed frame of reference, whereas, as indicated in Table 3, the wind tunnel data are measured relative to the flow direction. A transformation is therefore required, which is derived as follows. Let Ψ_f be the angle between the centreline of the ship and the flow direction (Fig. 10) and U_f and W_f be the streamwise and cross-stream velocities of the flow. Referring to Fig. 10, the transformation to the earth axes set (incorporating the downward component which is the same in both axes sets) will be given by

$$V_{a,g} = \begin{bmatrix} \dot{x}_w \\ \dot{y}_w \\ \dot{z}_w \end{bmatrix} = \begin{bmatrix} \cos\Psi_f & \sin\Psi_f & 0 \\ \sin\Psi_f & -\cos\Psi_f & 0 \\ 0 & 0 & 1 \end{bmatrix} \begin{bmatrix} U_f \\ W_f \\ V_f \end{bmatrix}$$

By selecting the appropriate runs from Table 2 and performing the transformation given previously, with $\Psi_f = 30°$, the wind data required can be converted to an appropriate form as shown in Table 4 subsequently.

The data from Table 4 are plotted in Fig. 11 and represent a useable wind distribution time history for the inverse simulation. The data presented in Table 4 and Fig. 11 is an average value taken over the 4 s measurement period during the wind tunnel test. The question of how so few points are to be used to generate a time history was given extensive consideration. For example, it is possible to fit a smooth polynomial profile through the time points to generate a continuous profile. Given that the wind data are actually a mean value of fluctuating turbulence, any form of smoothing would be unrepresentative, therefore, it was decided that simple linear variation between the points would be the most appropriate course of action. The final stage in preparing the wind data is to scale it to an appropriate intensity. For previous results, a 40 knot

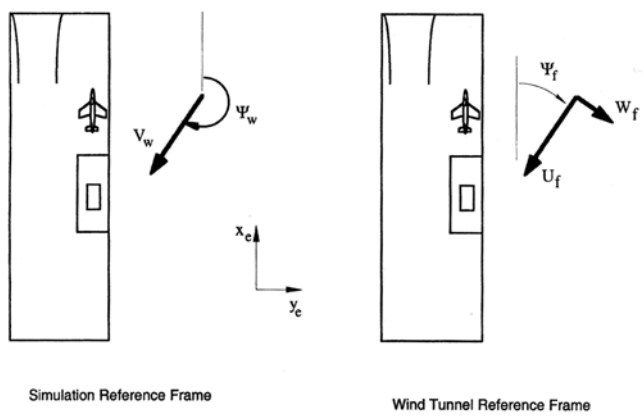

Fig. 10 Frames of reference for wind data

Table 4 Wind velocity information for landing manoeuvre

Run number	Lateral reference	Height reference	Time (s)	$\dot{x}_w$ (m/s)	$\dot{y}_w$ (m/s)	$\dot{z}_w$ (m/s)
89	6	1	0.0	11.436	7.315	2.816
86	5	1	6.8	9.52	7.214	1.463
49	1	1	13.01	11.068	8.068	−0.837
50	1	2	18.06	9.402	7.177	−1.492
81	1	3	19.56	7.062	4.226	−1.62

(20.59 m/s) mean wind speed was used, and hence, for consistency, the wind velocities presented in Table 4 and Fig. 11 (which measured at a freestream speed of 13.2 m/s) were scaled by a factor of 1.56.

6.3 Inverse simulation results

With the flight path model and wind distribution model both available, it is possible to simulate a Lynx helicopter performing the landing manoeuvre through the wind recorded in the wind tunnel experiments. The results are shown in Fig. 12, plotted in comparison with the still air results.

The results show that the presence of the wind does enforce changes to the amplitude of the control inputs (suggesting some increase in workload), but no gross change to the strategy adopted by the pilot. Although there is a clear offset in all of the controls, in each case there is still plenty of margin left, indicating that the helicopter will still be controllable in this environment. The rotorspeed does approach its limit during the initial descent phase of the landing due to the presence of a small up-gust at this time.

7 SIMULATION OF TRANSPORT HELICOPTER LANDING ON DECK AFT OF SUPERSTRUCTURE

Having repeated the aforementioned analysis for various locations on the deck, it was clear that the likely airwake conditions for ship of this design would cause little difficulty for small agile helicopter such as the Lynx. A significant feature of this aircraft is that it possesses a rotor which is stiff (i.e. hingeless) in its flap degree of freedom. This affords it superior control power and manoeuvrability over helicopters with flap hinged rotors. Clearly, a larger, less agile helicopter may not be as capable of landing safely in the modelled conditions. To illustrate this, a

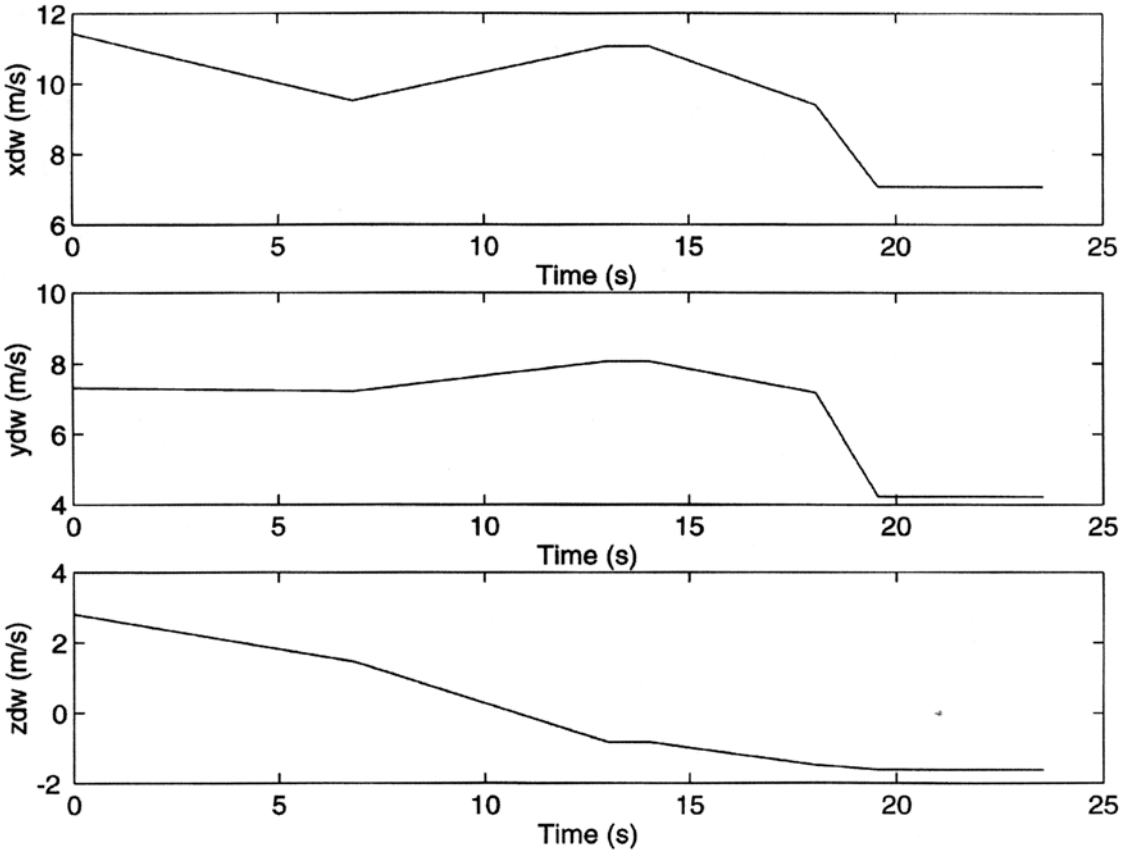

Fig. 11 Wind distribution from wind tunnel data

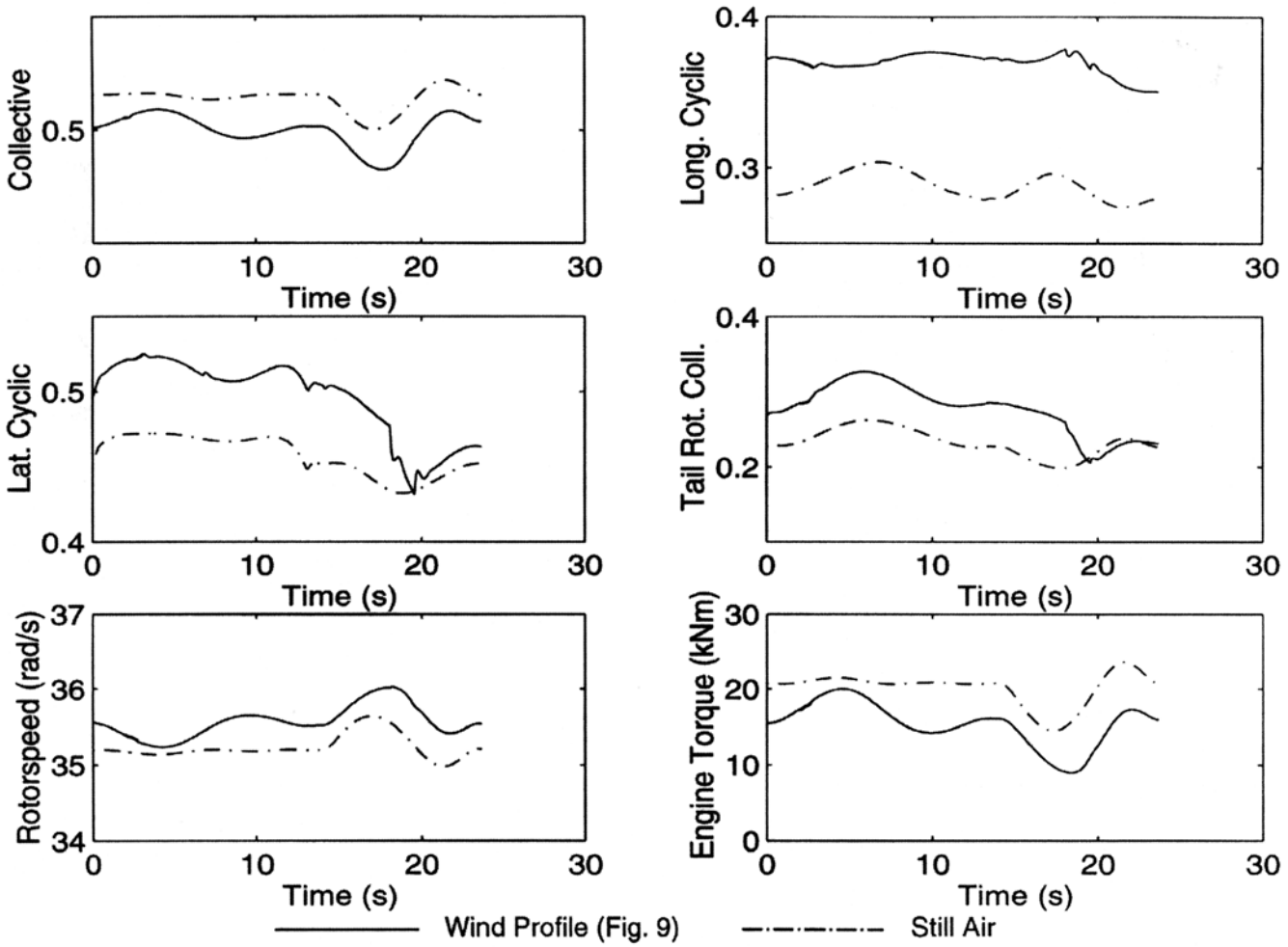

Fig. 12 Inverse simulation results for Lynx flying landing manoeuvre (data from points 6–5–1, mean wind speed of 40 knots)

different data set representing a larger transport helicopter of mass 8000 kg (based loosely on the Westland Sea King) was implemented in the HGS mathematical model. The inverse simulation of the transport helicopter flying the flight path as shown in Fig. 9, with the wind conditions given by Fig. 10 is shown in Fig. 13. This is directly comparable with the Lynx results shown in Fig. 12.

The plot for the collective channel shows that during the vertical descent stage, the collective pitch calculation estimates a value below zero. The wind profile used is shown in Fig. 10, and it can be seen that at the time of the control limit being exceeded, the helicopter is experiencing an up-gust of around 2 m/s. In fact, the control limit is exceeded for only a fraction of a second; however, this indicates that the transport helicopter would not be able to complete this manoeuvre in the defined manner. It is clear that there are configurational characteristics that can affect the ability of the helicopter to perform the manoeuvre.

Another issue relates to the manoeuvre model used. Although this model is representative of the type flown and should lead to realistic strategies being derived, there is the question of the parameters used – increasing or decreasing parameters vary, the severity of the manoeuvre and influence the predicted control strategy. For example, increasing the maximum sideward velocity in the sidestep phase from 10 knots to 20 knots increases the power and torque requirements, and in the presence of a sidewinds power and torque (engine and tail rotor) limits are quickly exceeded. The flight path parameters used in the current work were selected to generate relatively gentle manoeuvres well within the normal operating limits. If more aggressive piloting was the norm, then the choice of parameters would have to be reviewed to reflect this.

It should also be noted that there is an assumption inherent in the helicopter mathematical model that the whole rotor is immersed instantaneously in the gust field. In fact, there are penetration effects

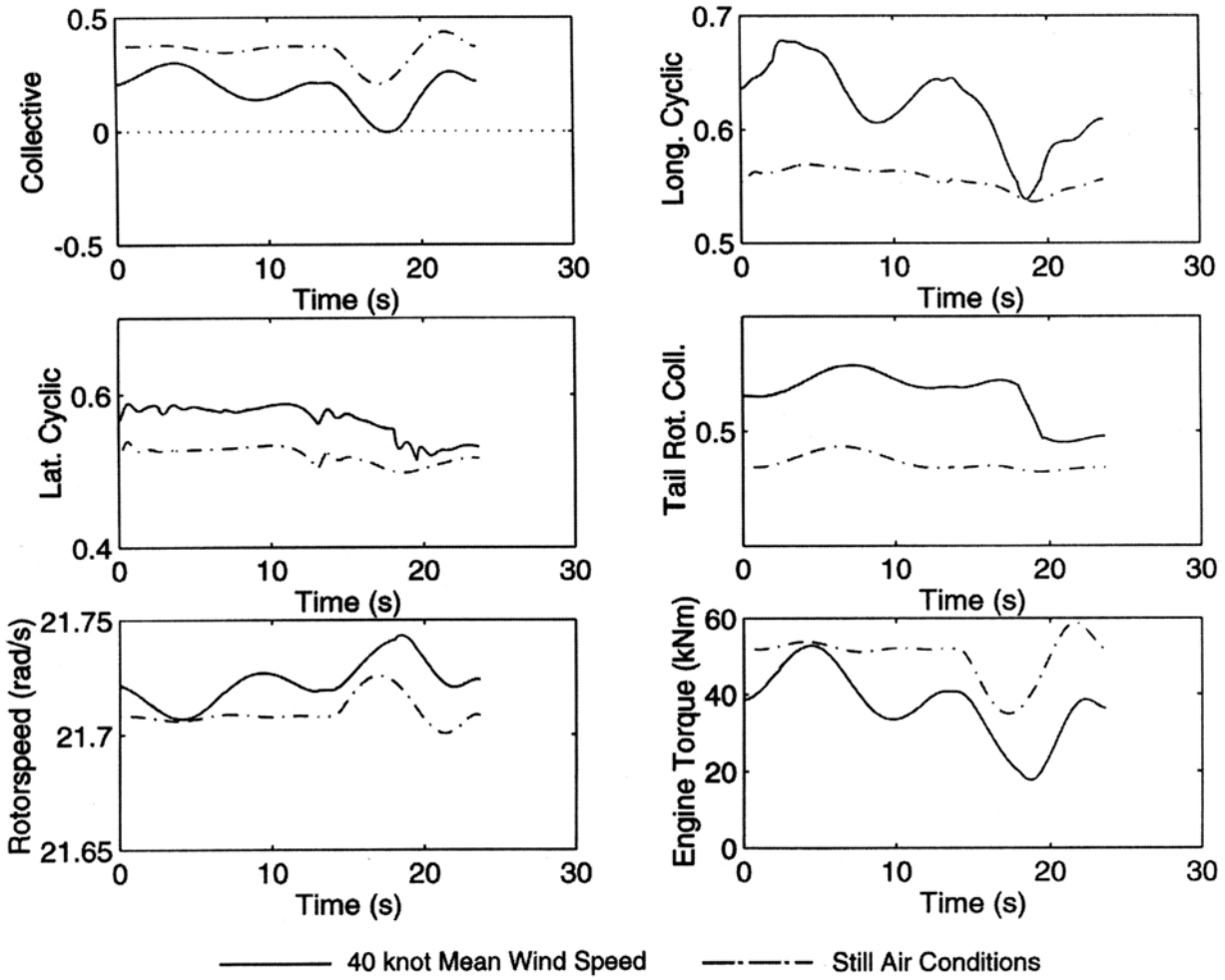

Fig. 13 Simulation of transport helicopter landing aft of superstructure

present (different regions of the rotor disc experiencing different flow speeds as the helicopter progresses through the manoeuvre). Such penetrations lead to load variations across the disc and generate high levels of vibration. A simulation such as the HGS model used here is unable to capture this effect, however, gust penetration can be incorporated into individual blade models. Research into inverse simulation using individual blade models (including gust penetration) is currently underway at Glasgow.

Finally, the way in which the wind data are processed may have an influence on the nature of the final results. The simulation requires time histories of the wind distribution, whereas the data provided from the wind tunnel were measured at discrete locations, with time histories of flow speeds at each location. The mean value at each location was used, and so, information on the rate of change of wind speed and turbulence is lost. Ideally, the measurement from the wind tunnel should be recorded in real time as the probe is traversed along the flight path to be simulated. This would represent a technical challenge but would generate a more realistic model of the wind.

8 CONCLUDING REMARKS

The construction of SHOL diagram is essential for safe and effective operation of a helicopter from a ship deck. This is a lengthy and expensive exercise, and consequently, any analytical aid which can reduce the number of flights required must be of value. In this report, the use of inverse simulation to achieve this goal has been demonstrated. It is clear that the technique can differentiate between acceptable and unacceptable performances in particular atmospheric conditions for specific helicopter configurations. Inverse simulation techniques are becoming well established and accepted, and so the real challenges in using this method are in ensuring that the helicopter model is representative and that the airwake data are realistic. The current

study also included wind tunnel testing of a contemporary helicopter carrier/assault ship design, which indicated that the most critical condition occurs when there is a wind coming from an angle of 30° from starboard across the superstructure. In these conditions, there is substantial recirculation region in the wake of the ship superstructure which could provide landing conditions outwith the normal operational boundaries of the helicopter. This work also demonstrates that wind tunnel data can be translated into a form suitable for use with inverse simulation. It is then clear that inverse simulation has the potential to contribute to the construction of the SHOL diagrams and thereby assists in determining the operational limits of the ship/helicopter combination.

ACKNOWLEDGEMENTS

The authors wish to acknowledge the support of Hanjin Hervy Industries who funded this study.

REFERENCES

1 **Gowen, T. E.** and **Ferrier, B.** Manned flight simulator shipborne handling qualities assessment using the proposed ADS-33 standard. In Proceedings of the 57th Annual Forum of the American Helicopter Society, Washington, DC, May 2001.
2 **Handcock, A., Lane, R., Johns, S., Howitt, J.,** and **Charlton, M.** Benefits of advanced control technology. In Proceedings of the 56th Annual Forum of the American Helicopter Society, Virginia Beach, May 2000.
3 **Lee, D., Sezer-Uzol, N., Horn, J. F.,** and **Long, L. N.** Simulation of helicopter shipboard launch and recovery with time accurate airwakes. *AIAA J. Aircraft*, 2005, **42**(2), 448–461.
4 **Celi, R.** Optimization-based inverse simulation of a helicopter slalom maneuver. In Proceedings of the 25th European Rotorcraft Forum, Rome, September 1999.
5 **Hess, R., Zeyada, Y.,** and **Heffley, R. K.** Modelling and simulation for helicopter task analysis. In Proceedings of the 57th Annual Forum of the American Helicopter Society, Washington, DC, May 2001.
6 **Avanzini, G.** and **de Matteis, G.** Two-timescale inverse simulation of a helicopter model. *AIAA J. Guid. Control Dynam.*, 2001, **24**(2), 330–339.
7 **Thomson, D. G.** and **Bradley, R.** The principles and practical application of helicopter inverse simulation. *Simulat. Theory Pract.*, 1998, **6**(1), 47–70.
8 **Rutherford, S.** and **Thomson, D. G.** Helicopter inverse simulation incorporating an individual blade rotor model. *AIAA J. Aircraft*, 1997, **34**(5), 627–634.
9 **Thomson, D. G.** and **Bradley, R.** The use of inverse simulation for preliminary assessment of helicopter handling qualities. *Aeronaut. J.*, 1997, **101**, 287–294.
10 **Thomson, D. G., Talbot, N., Taylor, C., Bradley, R.,** and **Ablett, R.** An investigation of piloting strategies for engine failures during take-off from offshore platforms. *Aeronaut. J.*, 1995, **99**(981), 15–25.
11 **Thomson, D. G.** Development of a generic helicopter mathematical model for application to inverse simulation. Internal report No. 9216, Department of Aerospace Engineering, University of Glasgow, June 1992.
12 **Thomson, D. G.** and **Bradley, R.** Mathematical modelling of helicopter manoeuvers. *J. Am. Helicopter Soc.*, 1997, **42**(4), 307–309.
13 **Padfield, G. D.** *Helicopter flight dynamics*, 2000 (Blackwell Science, Oxford).

APPENDIX

Notation

h	height of helicopter above ship deck at start of manoeuvre
I_{xx}, I_{yy}, I_{zz}, I_{xz}	moments and product of inertia
K_3	rotorspeed governor gain
L, M, N	external moments
m	aircraft mass
P, Q, R	roll, pitch, and yaw rates
Q_E	engine torque
s	helicopter's distance to port side of ship at start of manoeuvre
t	time
t_s	stabilization time
U, V, W	component translational velocities
U_f, W_f, V_f	flow components from wind tunnel tests
$\boldsymbol{V}$	velocity vector
V_f	flight velocity of helicopter
V_s	constant velocity of ship
V_w	mean wind speed
x_e, y_e, z_e	flight path coordinate positions
$\dot{x}_w$, $\dot{y}_w$, $\dot{z}_w$	wind velocity components in earth axes
X, Y, Z	external forces
$\dot{y}_{max}$	maximum sideward velocity in sidestep phase of landing
$\dot{z}_{max}$	maximum downward velocity in descent phase of landing
α_f, β_f	helicopter angles of attack and sideslip
Φ, Θ, Ψ	roll, pitch, and azimuth angles (the Euler angles)
Ψ_f	relative flow direction in wind tunnel tests
Ψ_w	wind heading (from north)
τ_{e_1}, τ_{e_2}, τ_{e_3}	rotorspeed governor time constants
θ_0	main rotor collective pitch

θ_{1s}, θ_{1c}	main rotor longitudinal and lateral cyclic pitch
θ_{0tr}	tail rotor collective pitch
Ω	main rotor angular speed
Ω_{idle}	angular velocity of the rotor in idle

Convention for control positions

Collective lever	0 = full down, 1 = full up
Lateral stick	0 = full left, 1 = full right
Longitudinal stick	0 = full aft, 1 = full forward
Pedal position	0 = full left, 1 = full right

Subscripts

a	air
g	ground
h	helicopter